Dalton Transactions

PAPER

View Article Online
View Journal | View Issue

Cite this: *Dalton Trans.*, 2015, **44**, 20392

Cyclometalated Ir(III) complexes of deprotonated *N*-methylbipyridinium ligands: effects of quaternised N centre position on luminescence†

Benjamin J. Coe,*[a] Madeleine Helliwell,[a] James Raftery,[a] Sergio Sánchez,[a] Martyn K. Peers[b] and Nigel S. Scrutton[b]

Received 25th September 2015,
Accepted 15th October 2015

DOI: 10.1039/c5dt03753k

www.rsc.org/dalton

Six new tricationic Ir^{III} complexes of cyclometalating ligands derived from 1-methyl-2-(2′-pyridyl)pyridinium or 1-methyl-4-(2′-pyridyl)pyridinium are described. These complexes of the form $[Ir^{III}(C^N)_2(N^N)]^{3+}$ (C^N = cyclometalating ligand; N^N = α-diimine) have been isolated and characterised as their PF_6^- and Cl^- salts. Four of the PF_6^- salts have been studied by X-ray crystallography, and structures have been obtained also for two complex salts containing MeCN and Cl^- or two Cl^- ligands instead of N^N. The influence of the position of the quaternised N atom in C^N and the substituents on N^N on the electronic/optical properties are compared with those of the analogous complexes where C^N derives from 1-methyl-3-(2′-pyridyl)pyridinium (B. J. Coe, *et al.*, *Dalton Trans.*, 2015, **44**, 15420). Voltammetric studies reveal one irreversible oxidation and multiple reduction processes which are mostly reversible. The new complexes show intramolecular charge-transfer absorptions between 350 and 450 nm, and exhibit bright green luminescence, with λ_{max} values in the range 508–530 nm in both aqueous and acetonitrile solutions. In order to gain insights into the factors that govern the emission properties, density functional theory (DFT) and time-dependent DFT calculations have been carried out. The results confirm that the emission arises largely from triplet excited states of the C^N ligand (^{3}LC), with some triplet metal-to-ligand charge-transfer (^{3}MLCT) contributions.

Introduction

Cyclometalated Ir^{III} complexes have attracted attention for many years, with a primary focus being their fascinating optical emission properties.[1–7] Such species show high stability, large quantum yields and long-lived excited states, due to strong spin–orbit coupling. Therefore, they are of interest for uses in a wide range of fields including organic light-emitting diodes (OLEDs),[8–10] light-emitting electrochemical cells,[11–13] chemosensors and biological imaging.[14–20] Most of the reported complexes fall into two classes; neutral homoleptic $Ir^{III}(C^N)_3$ and heteroleptic $Ir^{III}(C^N)_2(L–X)$ (C^N = cyclometalating ligand; L–X = monoanionic ancillary ligand),[8,9,21–32] and monocationic heteroleptic species $[Ir^{III}(C^N)_2(L–L)]^+$ (L–L = neutral bidentate ligand).[7,11–13,33–40] The emission properties of the latter are tuned readily, and various strategies have been adopted. These include changing the degree of π-conjugation in the ligands,[34] incorporating electron-rich S-heterocycles,[41–44] or most commonly, functionalising C^N or L–L to adjust the energies of the metal and ligand orbitals.[1,36,37,44] The electronic properties of substituents and their positioning with respect to the coordinating carbon of C^N influence greatly the energy of the emission.

In the context of luminescence, Ir^{III} complexes with C^N ligands derived from pyridinium species were apparently unknown until we reported those of deprotonated 1-methyl-3-(2′-pyridyl)pyridinium (3,2′-C^N).[45] The only previous account of structurally related species concerns catalytic studies with hydride complexes that are unsuitable for luminescence.[46] A number of reports of cyclometalated complexes of *N*-methylbipyridinium species with Pd/Pt[47] or Ru[48] have appeared. The bright blue or blue-green emission and aqueous solubility of our Ir^{III} 3,2′-C^N species[45] suggests potential uses in highly efficient OLEDs and/or bio-sensing/imaging. Since the use of Ir^{III} complexes in the latter context[16–20,49] is often restricted by poor water solubility,[19] increasing their charge from the usual +1 to +3 is beneficial. This structural novelty opens doors for designing further complexes of C^N ligands based on

[a]*School of Chemistry, The University of Manchester, Oxford Road, Manchester M13 9PL, UK. E-mail: b.coe@manchester.ac.uk*
[b]*Manchester Institute of Biotechnology, Faculty of Life Sciences, The University of Manchester, 131 Princess Street, Manchester M1 7DN, UK*

†Electronic supplementary information (ESI) available: Characterisation and theoretical studies. CCDC 1427669–1427674. For ESI and crystallographic data in CIF or other electronic format see DOI: 10.1039/c5dt03753k

quaternised bipyridinium units with attractive electronic and optical properties. In the previously published complexes $[Ir^{III}(C^N)_2(N^N)]^{3+}$ (N^N = α-diimine), both the nature and energy of the emission are highly influenced by substituents on the ancillary N^N ligand.[45] Density functional theory (DFT) calculations show that the blue emission observed when N^N = 2,2′-bipyridyl (bpy) or 4,4′-(^{t}Bu)$_2$bpy is mainly triplet ligand-centred (^{3}LC) with some triplet metal-to-ligand charge-transfer (^{3}MLCT) character from C^N. On the other hand, the blue-green emission observed when N^N = 4,4′-$(CF_3)_2$bpy has ^{3}L′C with some ^{3}ML′CT nature, due to efficient inter-ligand energy transfer to N^N (L′).

In addition to changing the substituents on N^N, it is of interest to study the effects on the emission properties of varying the location of the quaternised N centre in the C^N ligand. Here, we present a series of new Ir^{III} complexes related to those described recently, but with the C^N ligands derived instead from 1-methyl-2-(2′-pyridyl)pyridinium of 1-methyl-4-(2′-pyridyl)pyridinium. Using as the ancillary ligand bpy, 4,4′-(^{t}Bu)$_2$bpy or 4,4′-$(CF_3)_2$bpy allows detailed comparisons and reveals the importance of the position of the quaternised centre in achieving blue emission.

Experimental section

Materials and procedures

The compound 1-methyl-3-(2′-pyridyl)pyridinium hexafluorophosphate and the complex salts **4P–6P** and **4Cl–6Cl** were synthesised as described previously.[45] All other reagents were obtained commercially and used as supplied. Products were dried overnight in a vacuum desiccator (silica gel) prior to characterisation. In each case, the bold number refers to the complex cation, while the counter-anions are denoted by **P** for PF_6^- or **C** for Cl^-.

General physical measurements

^{1}H NMR spectra were recorded on a Bruker UltraShield AV-400 spectrometer, with all shifts referenced to residual solvent signals and quoted with respect to TMS. Elemental analyses were performed by the Microanalytical Laboratory, University of Manchester, and UV–vis spectra were obtained by using a Shimadzu UV-2401 PC spectrophotometer. Mass spectra were recorded by using +electrospray on a Micromass Platform II spectrometer. Cyclic voltammetric measurements were performed by using an Ivium CompactStat. A single-compartment cell was used with a silver/silver chloride reference electrode (3 M NaCl, saturated AgCl) separated by a salt bridge from a 2 mm disc platinum working electrode and platinum wire auxiliary electrode. Acetonitrile was used as supplied from Sigma-Aldrich (HPLC grade), and $[N^nBu_4]PF_6$ (Fluka, electrochemical grade) was used as the supporting electrolyte. Solutions containing *ca.* 1.5×10^{-4} M analyte (0.1 M $[N^nBu_4]PF_6$) were deaerated by purging with N_2. All $E_{1/2}$ values were calculated from $(E_{pa} + E_{pc})/2$ at a scan rate of 100 mV s^{-1}. Steady-state emission and excitation spectra were recorded on an Edinburgh Instruments FP920 Phosphorescence Lifetime Spectrometer equipped with a 5 W microsecond pulsed xenon flashlamp. Lifetime data were recorded following excitation with an EPL 375 picosecond pulsed diode laser (Edinburgh Instruments), using time-correlated single photon counting (PCS900 plug-in PC card for fast photon counting). Lifetimes were obtained by tail fitting on the data obtained, or by a reconvolution fit using a solution of Ludox® in the scatterer, and the quality of fit judged by minimisation of reduced chi-squared and residuals squared. Quantum yields were measured upon excitation at 420 nm by using a SM4 Integrating Sphere mounted on an Edinburgh Instruments FP920 Phosphorescence Lifetime Spectrometer.

Synthesis

1-Methyl-2-(2′-pyridyl)pyridinium iodide. Methyl iodide (2.4 mL, 38.6 mmol) was added to a solution of 2,2′-bipyridyl (2.00 g, 12.8 mmol) in acetonitrile (25 mL) and heated at 45 °C for 48 h under argon. After cooling to room temperature, the yellow precipitate of *N*,*N*′-dimethyl-2,2′-bipyridinium iodide was filtered off. The filtrate was poured into diethyl ether (200 mL) and after 5 min the precipitate was filtered off, washed with diethyl ether and dried to give an off-white powder: 1.81 g (47%). δ_H (400 MHz, CD_3OD) 9.10 (1 H, d, J = 6.1 Hz), 8.86 (1 H, d, J = 4.7 Hz), 8.71 (1 H, t, J = 7.6 Hz), 8.25 (1 H, d, J = 8.0 Hz), 8.19–8.14 (2 H), 7.95 (1 H, d, J = 7.9 Hz), 7.70 (1 H, ddd, J = 7.7, 4.8, 0.8 Hz), 4.37 (3 H, s). ES-MS: m/z = 171 $[M - I]^+$.

1-Methyl-4-(2′-pyridyl)pyridinium iodide. This compound was prepared in a manner identical to 1-methyl-3-(2′-pyridyl)-pyridinium iodide by using 2,4′-bipyridyl (500 mg, 3.20 mmol) in place of 2,2′-bipyridyl to give an off-white powder: 915 mg (96%). δ_H (400 MHz, CD_3OD) 8.98 (2 H, d, J = 6.8 Hz), 8.86 (1 H, ddd, J = 4.8, 1.8, 0.9 Hz), 8.77 (2 H, d, J = 6.9 Hz), 8.34 (1 H, dt, J = 8.0, 1.0 Hz), 8.08 (1 H, td, J = 7.8, 1.8 Hz), 7.63 (1 H, ddd, J = 7.7, 4.8, 1.0 Hz), 4.45 (3 H, s). ES-MS: m/z = 171 $[M - I]^+$.

1-Methyl-2-(2′-pyridyl)pyridinium hexafluorophosphate. 1-Methyl-2-(2′-pyridyl)pyridinium iodide was dissolved in a minimum of water and filtered to give a pale yellow solution to which solid NH_4PF_6 was added. The precipitate was filtered off and washed extensively with cold water to afford a white powder in near quantitative yield. δ_H (400 MHz, CD_3CN) 8.82 (1 H, d, J = 4.2 Hz), 8.73 (1 H, d, J = 6.3 Hz), 8.58 (1 H, t, J = 7.9 Hz), 8.11–8.04 (3 H), 7.77 (1 H, d, J = 7.9 Hz), 7.65 (1 H, ddd, J = 7.8, 4.8, 1.1 Hz), 4.23 (3 H, s). ES-MS: m/z = 171 $[M - PF_6]^+$. Anal. Calcd (%) for $C_{11}H_{11}F_6N_2P$: C, 41.8; H, 3.5; N, 8.9. Found: C, 42.0; H, 3.1; N 8.8.

1-Methyl-4-(2′-pyridyl)pyridinium hexafluorophosphate. This compound was prepared in a manner identical to 1-methyl-2-(2′-pyridyl)pyridinium hexafluorophosphate by using 1-methyl-4-(2′-pyridyl)pyridinium iodide to give a white powder. δ_H (400 MHz, CD_3CN) 8.83 (1 H, d, J = 4.7 Hz), 8.67 (2 H, d, J = 6.8 Hz), 8.62 (2 H, d, J = 6.7 Hz), 8.19 (1 H, d, J = 8.0 Hz), 8.04 (1 H, td, J = 7.8, 1.7 Hz), 7.60 (1 H, ddd, J = 7.6, 4.7, 0.9 Hz), 4.31 (3 H, s). ES-MS: m/z = 171 $[M - PF_6]^+$. Anal.

Calcd (%) for $C_{11}H_{11}F_6N_2P$: C, 41.8; H, 3.5; N, 8.9. Found: C, 42.0; H, 3.2; N 8.9.

$[\{Ir^{III}(2,2'\text{-}C\text{^}N)_2Cl\}_2][PF_6]_4$ [2,2′-C^N = cyclometalated anion derived from 1-methyl-2-(2′-pyridyl)pyridinium]. $Ir^{III}Cl_3{\cdot}2.9H_2O$ (200 mg, 0.570 mmol) and 1-methyl-2-(2′-pyridyl)pyridinium hexafluorophosphate (377 mg, 1.19 mmol) were added to argon-sparged 2-methoxyethanol (22 mL) and water (8 mL), and the mixture heated at 120 °C for 48 h under argon. After cooling to room temperature, the mixture was filtered. An excess of NH_4PF_6 was added to the filtrate, and the solvents evaporated. The residue was suspended in ice-cold water and the solid filtered off, rinsed with a small volume of cold water, then acetone/diethyl ether (1 : 3, 4 × 5 mL), and dried to give a bright red powder: 331 mg (68%). δ_H (400 MHz, CD_3CN) 10.20 (2 H, ddd, J = 5.7, 1.7, 0. 7 Hz), 8.51 (2 H, d, J = 8.4 Hz), 8.16 (2 H, ddd, J = 8.5, 7.6, 1.7 Hz), 8.10 (2 H, dd, J = 5.9, 0.8 Hz), 7.74 (2 H, ddd, J = 7.6, 5.7, 1.3 Hz), 7.26 (2 H, dd, J = 7.9, 1.2 Hz), 7.11 (2 H, dd, J = 7.9, 5.9 Hz), 4.58 (6 H, s).

$[\{Ir^{III}(4,2'\text{-}C\text{^}N)_2Cl\}_2][PF_6]_4$ [4,2′-C^N = cyclometalated anion derived from 1-methyl-4-(2′-pyridyl)pyridinium]. This compound was prepared in a manner identical to $[\{Ir^{III}(2,2'\text{-}C\text{^}N)_2Cl\}_2][PF_6]_4$ by using 1-methyl-4-(2′-pyridyl)pyridinium hexafluorophosphate to give a red powder: 318 mg (65%). δ_H (400 MHz, CD_3CN) 9.97 (2 H, ddd, J = 5.7, 1.6, 0.7 Hz), 8.33 (2 H, ddd, J = 8.1, 1.4, 0.7 Hz), 8.13 (2 H, td, J = 7.8, 1.6 Hz), 8.04 (2 H, d, J = 6.3 Hz), 7.98 (2 H, dd, J = 6.5, 1.7 Hz), 7.73 (2 H, ddd, J = 7.5, 5.8, 1.5 Hz) 7.18 (2 H, d, J = 1.6 Hz), 3.90 (6 H, s).

$[Ir^{III}(2,2'\text{-}C\text{^}N)_2(bpy)][PF_6]_3$, 1P. Argon-sparged 2-methoxyethanol/water (8 : 2, 15 mL) was added to $[\{Ir^{III}(1\text{-}Me\text{-}2,2'\text{-}bpy)_2Cl\}_2][PF_6]_4$ (100 mg, 0.058 mmol), 2,2′-bipyridyl (30 mg, 0.192 mmol) and $AgPF_6$ (37 mg, 0.146 mmol) under argon, and the mixture heated at 100 °C for 36 h. After cooling to room temperature, the solution was filtered through Celite to remove AgCl and the solvents evaporated. The residue was dissolved in a minimum volume of acetone and an excess of $[N^nBu_4]Cl$ added. The precipitate was filtered off, washed with acetone and purified by column chromatography on Sephadex SP C-25, eluting with 0.025–0.075 M NaCl in acetone/water (1 : 1). The main yellow band was evaporated to dryness, cold methanol was added and NaCl removed by filtration. The filtrate was evaporated to dryness, and the residue dissolved in cold water. NH_4PF_6 was added and the precipitate filtered off, washed with ice-cold water and dried to give a bright yellow powder: 77 mg (58%). δ_H (400 MHz, CD_3CN) 8.60 (4 H, d, J = 8.3 Hz), 8.42 (2 H, dd, J = 6.0, 0.9 Hz), 8.26 (2 H, td, J = 8.0, 1.5 Hz), 8.19 (2 H, ddd, J = 8.6, 7.7, 1.6 Hz), 7.94 (2 H, ddd, J = 5.5, 1.5, 0.7 Hz), 7.90 (2 H, ddd, J = 5.7, 1.6, 0.6 Hz), 7.57 (2 H, ddd, J = 7.7, 5.5, 1.3 Hz) 7.46 (2 H, ddd, J = 7.7, 5.7, 1.2 Hz), 7.38 (2 H, dd, J = 7.9, 6.0 Hz), 7.21 (2 H, dd, J = 7.9, 1.3 Hz), 4.65 (6 H, s). ES-MS: m/z = 417 $[M - 2PF_6]^{2+}$, 344 $[M - 3PF_6]^{2+}$, 230 $[M - 3PF_6]^{3+}$. Anal. Calcd (%) for $C_{32}H_{28}F_{18}IrN_6P_3{\cdot}H_2O$: C, 33.7; H, 2.6; N, 7.4. Found: C, 33.8; H, 2.3; N, 7.3.

$[Ir^{III}(2,2'\text{-}C\text{^}N)_2\{4,4'\text{-}(CF_3)_2bpy\}][PF_6]_3$, 2P. This compound was prepared and purified in a manner identical to **1P** by using 4,4′-di-(trifluoromethyl)-2,2′-bipyridyl (56 mg, 0.192 mmol) in place of 2,2′-bipyridyl. A yellow powder was obtained: 71 mg (49%). δ_H (400 MHz, CD_3CN) 9.04 (2 H, s), 8.62 (2 H, d, J = 8.5 Hz), 8.45 (2 H, dd, J = 6.1, 0.9 Hz), 8.23–8.19 (4 H), 7.91–7.87 (4 H), 7.47 (2 H, ddd, J = 7.7, 5.8, 1.2 Hz), 7.41 (2 H, dd, J = 7.9, 6.0 Hz), 7.18 (2 H, dd, J = 7.9, 1.2 Hz), 4.66 (6 H, s). ES-MS: m/z = 1115 $[M - PF_6]^+$, 485 $[M - 2PF_6]^{2+}$, 275 $[M - 3PF_6]^{3+}$. Anal. Calcd (%) for $C_{34}H_{26}F_{24}IrN_6P_3$: C, 32.4; H, 2.1; N, 6.7. Found: C, 32.3; H, 1.6; N, 6.7.

$[Ir^{III}(2,2'\text{-}C\text{^}N)_2\{4,4'\text{-}(^tBu)_2bpy\}][PF_6]_3$, 3P. This compound was prepared in a manner identical to **1P** by using 4,4′-di-(*tert*-butyl)-2,2′-bipyridyl (52 mg, 0.194 mmol) in place of 2,2′-bipyridyl. A yellow powder was obtained: 85 mg (59%). δ_H (400 MHz, CD_3CN) 8.61 (2 H, d, J = 8.6 Hz), 8.54 (2 H, d, J = 1.7 Hz), 8.42 (2 H, dd, J = 6.0, 0.9 Hz), 8.19 (2 H, ddd, J = 8.6, 7.7, 1.5 Hz), 7.88 (2 H, dd, J = 5.7, 1.0 Hz), 7.79 (2 H, d, J = 5.9 Hz), 7.51–7.46 (4 H), 7.37 (2 H, dd, J = 7.9, 6.0 Hz), 7.21 (2 H, dd, J = 7.9, 1.1 Hz), 4.65 (6 H, s), 1.42 (18 H, s). ES-MS: m/z = 1092 $[M - PF_6]^+$, 472 $[M - 2PF_6]^{2+}$, 267 $[M - 3PF_6]^{3+}$. Anal. Calcd (%) for $C_{40}H_{44}F_{18}IrN_6P_3$: C, 38.9; H, 3.6; N, 6.8. Found: C, 38.4; H, 3.1; N, 6.5.

Compounds **7P–9P** were prepared and purified in a manner identical to **1P–3P** by reacting the appropriate ligands with $[\{Ir^{III}(4,2'\text{-}C\text{^}N)_2Cl\}_2][PF_6]_4$ instead of $[\{Ir^{III}(2,2'\text{-}C\text{^}N)_2Cl\}_2][PF_6]_4$.

$[Ir^{III}(4,2'\text{-}C\text{^}N)_2(bpy)][PF_6]_3$, 7P. Bright yellow powder: 73 mg (55%). δ_H (400 MHz, CD_3CN) 8.59 (2 H, d, J = 8.2 Hz), 8.44 (2 H, d, J = 8.0 Hz), 8.32 (2 H, d, J = 6.6 Hz), 8.27–8.23 (4 H), 8.16 (2 H, t, J = 8.2 Hz), 8.01 (2 H, d, J = 5.6 Hz), 7.73 (2 H, d, J = 5.6 Hz), 7.56 (2 H, t, J = 6.7 Hz), 7.44 (2 H, t, J = 6.7 Hz), 7.26 (2 H, s), 4.01 (6 H, s). ES-MS: m/z = 979 $[M - PF_6]^+$, 417 $[M - 2PF_6]^{2+}$, 230 $[M - 3PF_6]^{3+}$. Anal. Calcd (%) for $C_{32}H_{28}F_{18}IrN_6P_3{\cdot}H_2O$: C, 33.7; H, 2.6; N, 7.4. Found: C, 33.7; H, 2.4; N, 7.3.

$[Ir^{III}(4,2'\text{-}C\text{^}N)_2\{4,4'\text{-}(CF_3)_2bpy\}][PF_6]_3$, 8P. Yellow powder: 63 mg (43%). δ_H (400 MHz, CD_3CN) 9.03 (2 H, d, J = 0.7 Hz), 8.45 (2 H, dd, J = 8.2, 0.7 Hz), 8.35 (2 H, dd, J = 6.4, 1.0 Hz), 8.28 (2 H, d, J = 5.7 Hz), 8.27 (2 H, d, J = 6.4 Hz), 8.18 (2 H, td, J = 7.9, 1.4 Hz), 7.88 (2 H, dd, J = 5.8, 1.2 Hz), 7.75 (2 H, ddd, J = 5.8, 1.4, 0.7 Hz), 7.45 (2 H, ddd, J = 7.6, 5.9, 1.6 Hz), 7.23 (2 H, s), 4.02 (6 H, s). ES-MS: m/z = 412 $[M - 3PF_6]^{2+}$, 275 $[M - 3PF_6]^{3+}$. Anal. Calcd (%) for $C_{34}H_{26}F_{24}IrN_6P_3$: C, 32.4; H, 2.1; N, 6.7. Found: C, 32.3; H, 1.7; N, 6.6.

$[Ir^{III}(4,2'\text{-}C\text{^}N)_2\{4,4'\text{-}(^tBu)_2bpy\}][PF_6]_3$, 9P. Yellow powder: 45 mg (31%). δ_H (400 MHz, CD_3CN) 8.53 (2 H, d, J = 1.7 Hz), 8.44 (2 H, d, J = 8.1 Hz), 8.31 (2 H, dd, J = 6.5, 1.4 Hz), 8.25 (2 H, d, J = 6.4 Hz), 8.16 (2 H, td, J = 7.9, 1.4 Hz), 7.88 (2 H, d, J = 5.9 Hz), 7.72 (2 H, d, J = 5.9 Hz), 7.72 (2 H, d, J = 5.8 Hz), 7.50–7.45 (4 H), 7.25 (2 H, s), 4.01 (6 H, s), 1.42 (18 H, s). ES-MS: m/z = 1091 $[M - PF_6]^+$, 472 $[M - 2PF_6]^{2+}$, 267 $[M - 3PF_6]^{3+}$. Anal. Calcd (%) for $C_{40}H_{44}F_{18}IrN_6P_3{\cdot}H_2O$: C, 38.3; H, 3.7; N, 6.7. Found: C, 38.1; H, 3.6; N, 6.8.

$[Ir^{III}(2,2'\text{-}C\text{^}N)_2(bpy)]Cl_3$, 1C. To a solution of **1P** in acetone was added an excess of $[N^nBu_4]Cl$. The precipitate was filtered off, washed with acetone then diethyl ether and dried to give a near quantitative yield of a pale yellow solid. δ_H (400 MHz, $(CD_3)_2SO$) 8.99 (2 H, d, J = 8.4 Hz), 8.90 (2 H, d, J = 5.1 Hz),

8.86 (2 H, d, J = 8.6 Hz), 8.37 (2 H, td, J = 7.9, 1.4 Hz), 8.29 (2 H, td, J = 8.2, 1.4 Hz), 7.99 (4 H), 7.66 (2 H, ddd, J = 7.5, 5.6, 1.2 Hz), 7.60–7.56 (4 H), 7.17 (2 H, dd, J = 7.8, 0.9 Hz), 4.80 (6 H, s). ES-MS: m/z = 344 $[M - 3Cl]^{2+}$, 230 $[M - 3Cl]^{3+}$. Anal. Calcd (%) for $C_{32}H_{28}Cl_3IrN_6{\cdot}4H_2O$: C, 44.3; H, 4.2; N, 9.7. Found: C, 44.1; H, 4.0; N, 9.5.

$[Ir^{III}(2,2'\text{-}C\hat{}N)_2\{4,4'\text{-}(CF_3)_2bpy\}]Cl_3$, 2C. This compound was prepared in a manner identical to **1C** by using **2P** instead of **1P**. δ_H (400 MHz, $(CD_3)_2SO$) 9.70 (2 H, s), 8.96 (2 H, d, J = 5.6 Hz), 8.87 (2 H, d, J = 8.8 Hz), 8.31–8.28 (4 H), 8.08 (2 H, d, J = 5.4 Hz), 8.03 (2 H, d, J = 4.9 Hz), 7.61 (2 H, t, J = 6.9 Hz), 7.56 (2 H, t, J = 6.3 Hz), 7.05 (2 H, d, J = 7.9 Hz), 4.82 (6 H, s). ES-MS: m/z = 895 $[M - Cl]^+$, 430 $[M - 2Cl]^{2+}$, 413 $[M - 3Cl]^{2+}$, 275 $[M - 3Cl]^{3+}$. Anal. Calcd (%) for $C_{34}H_{26}Cl_3F_6IrN_6{\cdot}2H_2O$: C, 42.2; H, 3.1; N, 8.7. Found: C, 42.2; H, 3.0; N, 8.4.

$[Ir^{III}(2,2'\text{-}C\hat{}N)_2\{4,4'\text{-}(^tBu)_2bpy\}]Cl_3$, 3C. This compound was prepared in a manner identical to **1C** by using **3P** instead of **1P**. δ_H (400 MHz, $(CD_3)_2SO$) 9.00 (2 H, s), 8.92 (2 H, d, J = 5.9 Hz), 8.87 (2 H, d, J = 8.7 Hz), 8.30 (2 H, t, J = 8.2 Hz), 7.96 (2 H, d, J = 5.2 Hz), 7.87 (2 H, d, J = 5.9 Hz), 7.63–7.56 (6 H), 7.07 (2 H, d, J = 7.9 Hz), 4.81 (6 H, s), 1.42 (18 H, s). ES-MS: m/z = 400 $[M - 3Cl]^{2+}$, 267 $[M - 3Cl]^{3+}$. Anal. Calcd (%) for $C_{40}H_{44}Cl_2IrN_6{\cdot}2.5H_2O$: C, 50.4; H, 5.2; N, 8.8. Found: C, 50.2; H, 5.6; N, 8.8.

$[Ir^{III}(4,2'\text{-}C\hat{}N)_2(bpy)]Cl_3$, 7C. This compound was prepared in a manner identical to **1C** by using **7P** instead of **1P**. δ_H (400 MHz, $(CD_3)_2SO$) 8.98 (2 H, d, J = 8.2 Hz), 8.84 (2 H, d, J = 8.2 Hz), 8.79 (2 H, d, J = 6.5 Hz), 8.74 (2 H, d, J = 6.4 Hz), 8.37 (2 H, td, J = 8.0, 1.3 Hz), 8.29 (2 H, td, J = 7.9, 1.3 Hz), 8.08 (2 H, d, J = 5.5 Hz), 7.80 (2 H, d, J = 5.5 Hz), 7.67 (2 H, td, J = 6.6, 0.8 Hz), 7.56–7.53 (4 H), 4.11 (6 H, s). ES-MS: m/z = 362 $[M - 2Cl]^{2+}$, 344 $[M - 3Cl]^{2+}$, 230 $[M - 3Cl]^{3+}$. Anal. Calcd (%) for $C_{32}H_{28}Cl_3IrN_6{\cdot}2H_2O$: C, 46.2; H, 3.9; N, 10.1. Found: C, 45.9; H, 3.8; N, 10.0.

$[Ir^{III}(4,2'\text{-}C\hat{}N)_2\{4,4'\text{-}(CF_3)_2bpy\}]Cl_3$, 8C. This compound was prepared in a manner identical to **1C** by using **8P** instead of **1P**. δ_H (400 MHz, $(CD_3)_2SO$) 9.67 (2 H, s), 8.82 (4 H, t, J = 8.0 Hz), 8.74 (2 H, d, J = 6.5 Hz), 8.38 (2 H, d, J = 5.8 Hz), 8.30 (2 H, t, J = 7.3 Hz), 8.03 (2 H, d, J = 5.8 Hz), 7.90 (2 H, d, J = 5.4 Hz), 7.52 (2 H, t, J = 6.7 Hz), 7.46 (2 H, s), 4.11 (6 H, s). ES-MS: m/z = 895 $[M - Cl]^+$, 430 $[M - 2Cl]^{2+}$, 413 $[M - 3Cl]^{2+}$, 275 $[M - 3Cl]^{3+}$. Anal. Calcd (%) for $C_{34}H_{26}Cl_3F_6IrN_6{\cdot}2H_2O$: C, 42.2; H, 3.1; N, 8.7. Found: C, 42.4; H, 3.2; N, 8.6.

$[Ir^{III}(4,2'\text{-}C\hat{}N)_2\{4,4'\text{-}(^tBu)_2bpy\}]Cl_3$, 9C. This compound was prepared in a manner identical to **1C** by using **9P** instead of **1P**. δ_H (400 MHz, $(CD_3)_2SO$) 8.95 (2 H, d, J = 1.6 Hz), 8.82 (2 H, d, J = 7.9 Hz), 8.77 (2 H, d, J = 6.3 Hz), 8.70 (2 H, d, J = 6.4 Hz), 8.30 (2 H, td, J = 7.9, 1.3 Hz), 7.94 (2 H, d, J = 6.0 Hz), 7.77 (2 H, d, J = 5.8 Hz), 7.60–7.56 (4 H), 7.49 (2 H, s), 4.10 (6 H, s), 1.42 (18 H, s). ES-MS: m/z = 400 $[M - 3Cl]^{2+}$, 267 $[M - 3Cl]^{3+}$. Anal. Calcd (%) for $C_{40}H_{44}Cl_2IrN_6{\cdot}3.5H_2O$: C, 49.5; H, 5.3; N, 8.7. Found: C, 49.5; H, 5.4; N, 8.7.

X-Ray crystallography

Single crystals of **1P**·1.5Me_2CO·0.25Et_2O, **3P**·4MeCN and **7P**·MeCN·Et_2O were grown by slow diffusion of diethyl ether vapour into solutions in acetone or acetonitrile. For **2P**·2$C_4H_8O_2$, slow evaporation of an acetonitrile/1,4-dioxane solution was used. An attempt to grow crystals of the dimeric precursor $[\{Ir^{III}(2,2'\text{-}C\hat{}N)_2Cl\}_2][PF_6]_4$ by slow evaporation of a nitromethane/MeCN solution gave instead the monometallic compound $[Ir^{III}(2,2'\text{-}C\hat{}N)_2Cl(MeCN)][PF_6]_2{\cdot}MeNO_2$ (**10P**·$MeNO_2$), while $[Ir^{III}(4,2'\text{-}C\hat{}N)_2Cl_2]PF_6{\cdot}2MeNO_2{\cdot}C_4H_8O_2$ (**11P**·2$MeNO_2$·$C_4H_8O_2$) was obtained when attempting to crystallise $[\{Ir^{III}(4,2'\text{-}C\hat{}N)_2Cl\}_2][PF_6]_4$ by slow evaporation of a nitromethane/1,4-dioxane solution. Data were collected on Oxford Diffraction XCalibur 2 or Bruker APEX CCD X-ray diffractometers by using MoKα radiation (λ = 0.71073 Å), and processed by using the Oxford Diffraction CrysAlis Pro or Bruker SMART software packages. The structures were solved by direct methods by using SIR-2004 [50] or SHELXS-97,[51] and refined by full-matrix least-squares on all data by using SHELXL-97. All other calculations were carried out by using the SHELXTL package.[52]

All non-hydrogen atoms were refined anisotropically (except for those of a disordered solvent molecule in **1P**·1.5Me_2CO·0.25Et_2O) and hydrogen atoms were included in idealised positions by using the riding model, with thermal parameters 1.2 times those of aromatic parent carbon atoms, and 1.5 times those of methyl parent carbons. The asymmetric unit of **1P**·1.5Me_2CO·0.25Et_2O contains the complex cation, three disordered PF_6^- anions, an ordered acetone molecule, a disordered acetone at 0.5 occupancy and a disordered diethyl ether molecule at 0.25 occupancy. All non-H atoms were refined anisotropically, except for the disordered diethyl ether; some restraints were applied for the disordered atoms. H atoms were included in calculated positions, except those of the disordered diethyl ether, which were omitted. The asymmetric unit of **2P**·2$C_4H_8O_2$ contains the complex cation, three PF_6^- anions and two 1,4-dioxane molecules. The C–O distances in one 1,4-dioxane molecule had to be restrained to 1.4 Å and the displacement parameters for the six ring atoms were refined by using the RIGU and DELU commands. The asymmetric unit of **3P**·4MeCN contains the complex cation, three PF_6^- anions, one of which is disordered, and four acetonitrile molecules, three of which are disordered. Restraints were applied to the F atoms of the disordered PF_6^-. Crystallographic data and refinement details are presented in Table 1.

Theoretical studies

DFT and time-dependent DFT (TD-DFT) calculations were undertaken on the complex cations **1–3** and **7** by using Gaussian 09.[53] Geometry optimisations of the singlet ground (S_0) and first triplet excited (T_1) states and subsequent TD-DFT calculations were carried out by using the M06 functional[54] with the Def2-QZVP[55,56] basis set and pseudopotential on Ir and Def2-SVP[57] on all other atoms. MeCN was used as CPCM solvent model.[58,59] Using these parameters, the first 100 excited singlet states were calculated and simulated UV–vis absorption spectra were convoluted with Gaussian curves of fwhm 3000 cm^{-1} by using GaussSum.[60]

Table 1 Crystallographic data and refinement details for solvates of the complex salts **1P–3P**, **7P**, **10P** and **11P**

	1P·1.5Me_2CO·0.25Et_2O	**2P**·2$C_4H_8O_2$	**3P**·4MeCN	**7P**·MeCN·Et_2O	**10P**·$MeNO_2$	**11P**·2$MeNO_2$·$C_4H_8O_2$
Empirical formula	$C_{37.50}H_{39.50}F_{18}IrN_6O_{1.75}P_3$	$C_{42}H_{42}F_{24}IrN_6O_4P_3$	$C_{48}H_{56}F_{18}IrN_{10}P_3$	$C_{38}H_{41}F_{18}IrN_7OP_3$	$C_{25}H_{26}ClF_{12}IrN_6O_2P_2$	$C_{28}H_{34}Cl_2F_6IrN_6O_6P$
FW	1229.38	1435.92	1400.14	1238.89	960.11	958.68
Crystal appearance	Yellow plate	Yellow block	Yellow plate	Green block	Orange rod	Violet block
Crystal system	Triclinic	Monoclinic	Triclinic	Monoclinic	Triclinic	Monoclinic
Space group	*P*$\bar{1}$	*C*2/*c*	*P*$\bar{1}$	*P*2$_1$/*n*	*P*$\bar{1}$	*P*2$_1$/*n*
a/Å	13.3456(19)	14.2871(4)	12.2738(19)	12.2122(7)	8.9237(12)	13.8628(7)
b/Å	13.3584(19)	19.2131(5)	12.369(2)	21.6961(12)	12.9355(18)	11.1945(6)
c/Å	13.788(2)	37.1997(9)	19.218(3)	17.2606(9)	15.352(2)	22.7606(11)
α/°	70.073(2)	90	98.396(3)	90	72.425(2)	90
β/°	87.824(3)	93.462(1)	101.854(3)	101.776(1)	82.518(3)	94.945(2)
γ/°	80.281(2)	90	97.282(2)	90	72.619(2)	90
U/Å^3	2277.2(6)	10 192.7(5)	2787.3(8)	4477.1(4)	1610.7(4)	3519.0(3)
Z	2	8	2	4	1	4
T/K	100(2)	100(2)	100(2)	100(2)	100(2)	180(2)
μ/mm^{-1}	3.152	7.200	2.586	3.207	4.433	9.906
Cryst size/mm	0.55 × 0.40 × 0.20	0.19 × 0.15 × 0.08	0.45 × 0.40 × 0.10	0.40 × 0.30 × 0.20	0.45 × 0.20 × 0.20	0.17 × 0.15 × 0.12
Reflns collected	13 319	34 713	16 345	25 575	9396	15 947
Independent reflns (R_{int})	9112 (0.0162)	8853 (0.0470)	11 170 (0.0196)	9101 (0.0330)	6387 (0.0158)	6493 (0.0623)
θ_{max}/° (completeness)	25.00 (98.3)	66.59 (98.4)	26.44 (97.2)	25.00 (99.6)	26.41 (96.6)	67.00 (96.2)
Reflns with $I > 2\sigma(I)$	8651	8415	10 511	7424	6080	5993
GOF on F^2	1.042	1.072	1.025	1.013	1.067	1.019
Final R_1, wR_2 [$I > 2\sigma(I)$]	0.0314, 0.0818	0.0380, 0.0944	0.0311, 0.0765	0.0377, 0.0845	0.0331, 0.0844	0.0595, 0.1665
(All data)	0.0332, 0.0831	0.0401, 0.0958	0.0337, 0.0780	0.0500, 0.0902	0.0352, 0.0857	0.0621, 0.1703
Peak and hole/eÅ^{-3}	1.754, −0.798	1.51, −1.10	1.726, −1.258	1.356, −0.731	1.705, −0.934	2.369, −1.658

Results and discussion

Synthesis and characterisation

The new complexes **1–3** and **7–9** (Fig. 1) were synthesised by following the procedure used previously for **4–6**.[45] The cyclometalated chloride-bridged dimeric intermediates were isolated in crude form only, but identified by ^{1}H NMR spectroscopy. Reacting these dimers with the appropriate N^N ligand in the presence of $AgPF_6$ affords the hexafluorophosphate salts **1P–3P** and **7P–9P** which were isolated after purification by column chromatography on Sephadex SP C-25. Yields are in the range *ca.* 30–60%. The chloride salts **1C–3C** and **7C–9C** were prepared in near quantitative yields by anion metathesis with [N^{n}Bu$_4$]Cl in acetone. The identities and purities of the new complex salts are confirmed by ^{1}H NMR spectroscopy, elemental analyses and +electrospray mass spectrometry, and in several cases also by X-ray crystallography (see below). Portions of representative ^{1}H NMR spectra for the bpy-containing complex salts **1P**, **4P** and **7P** are depicted in Fig. 2, showing large changes as the position of the quaternised N atom varies.

In order to further characterise the system, ^{13}C NMR experiments were carried out for selected compounds **1P**, **4P** and **7P** in CD_3CN (see the ESI, Table S1†). The signals were assigned *via* HMQC and HMBC spectroscopy. As expected, the ^{13}C NMR signals arising from the cyclometalating ring show the most variability as the quaternised N atom moves around. Notably, the cyclometalated carbon atom in **4P** (175.08 ppm) is deshielded when compared with **1P** (157.05 ppm) and **7P** (161.66 ppm). This difference is attributed to the electron-withdrawing effect of the quaternised N atom located in the *para*-position in **4P**. The observed low field chemical shift is similar to those found for the carbenic carbon atom in related Ir^{III} complexes of N-heterocyclic carbene ligands,[49b,61–64] and gives an indication of the carbene-like character of the cyclometalated C atom in complexes **4–6**.

Structural studies

Single crystals were obtained for solvated forms of **1P–3P** and **7P**, and also unexpectedly for the chloride complexes in **10P** and **11P**. Crystallographic data and refinement details are summarised in Table 1. Representions of the molecular structures of the complex cations are shown in Fig. 3, and selected distances and angles are presented in Table 2. The structures of solvates of **4P** and **6P** have been reported previously,[45] and data are included here for comparison purposes.

All of the tris-chelate complexes in **1P–4P**, **6P** and **7P** exhibit a pseudooctahedral geometry around the Ir centre with two cyclometalating bipyridinium ligands and one bidentate bpy, 4,4′-(^{t}Bu)$_2$bpy or 4,4′-(CF$_3$)$_2$bpy ligand. The strong *trans* effects of the C-donor fragments affect the structures in two important ways. First, these units adopt a *cis* geometry, so the pyridyl rings of the C^N ligands are *trans* disposed. Second, the Ir–N distances to the N^N ligand are extended by *ca.* 0.07–0.09 Å when compared with those to the C^N ligand in all cases, except for one of the independent complexes in **4P**. The Ir–N

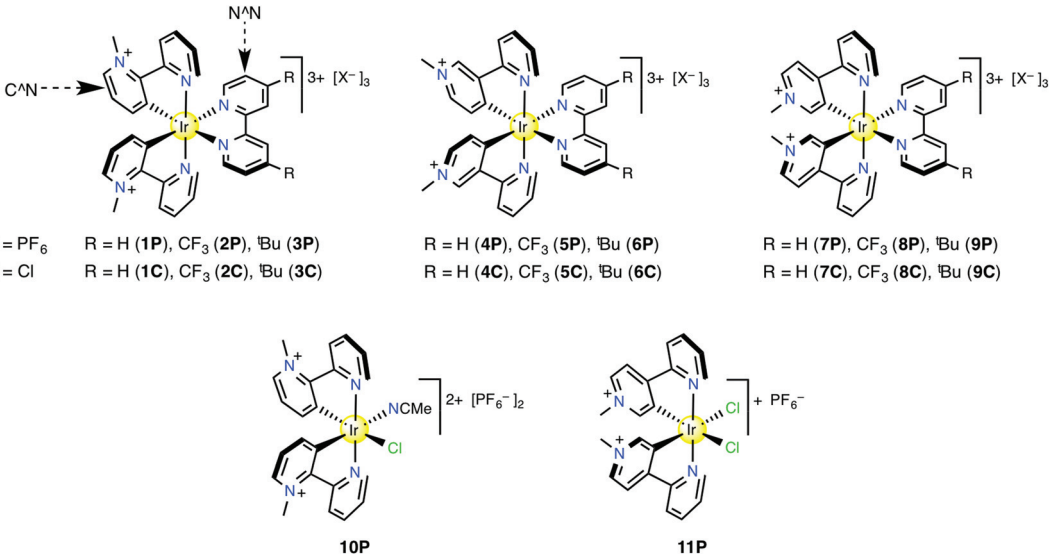

Fig. 1 Structures of the studied tris-chelate complex salts and the bis-chelates characterised by X-ray crystallography only.

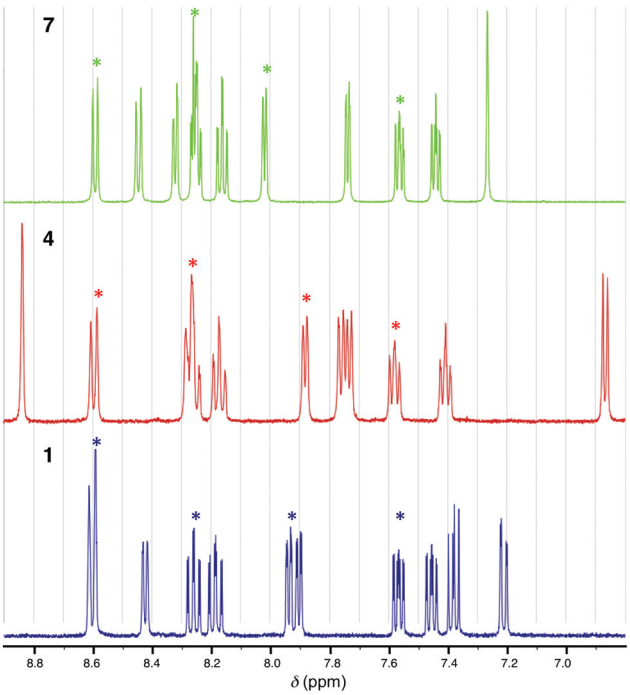

Fig. 2 Aromatic regions of the ^{1}H NMR spectra of the PF_6^- salts of complexes **1** (blue), **4** (red), and **7** (green) recorded at 400 MHz in CD_3CN. The asterisks denote the signals attributed *via* COSY studies to the protons of the N^N ligand.

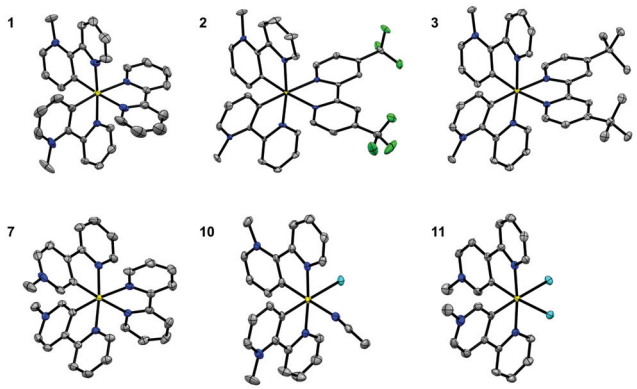

Fig. 3 Representations of the molecular structures of the solvates of **1P–3P**, **7P**, **10P** and **11P** with the anions, solvent molecules and H atoms removed for clarity (50% probability ellipsoids). Element colours: C = grey; N = blue; F = green; Cl = cyan; Ir = yellow.

distances to the N^N ligand are not affected significantly by varying the R substituents. The bite angle of N^N is essentially constant at *ca.* 77°, while that of the C^N ligand ranges from *ca.* 82–89°. Inspection of the bond distances within the cyclometalating rings does not reveal any clear evidence for quinoidal character in **4P** or **6P** that might be expected due to their carbene-like nature indicated by other physical measurements. The structures broadly resemble those reported for related monocationic Ir^{III} complexes, although the C^N bite angles are a little larger than those observed typically (*ca.* 80–81°).[34,36,39,65]

The fortuitously obtained structure of **11P** is relatively unusual. Various chloride-bridged dimeric Ir^{III} complexes with C^N derived from 2-phenylpyridine (ppy) or its derivatives have been characterised crystallographically.[66] However, apparently the only reported structure of a related monometallic dichloride complex is that of cyclometalated 2-(2,4-difluorophenyl)pyridine, crystallised as a monoanion with the cation $[Ir^{III}(C^N)_2(bpym)]^+$ (bpym = 2,2′-bipyrimidine) containing the same ligand.[67] The average Ir–Cl distance in this known compound of 2.493(4) Å is slightly longer than the corresponding distance in **11P** (2.464(1) Å, Table 2). Several neutral complexes $Ir^{III}(C^N)_2Cl(MeCN)$ have been reported previously,[66a,68]

Table 2 Selected geometric parameters for solvates of the complex salts **1P–4P**, **6P**, **7P**, **10P** and **11P**

Salt	**1P**	**2P**	**3P**	**4P**[a,b]		**6P**[a]	**7P**	**10P**	**11P**
Distances (Å)									
Ir–C	2.002(4)	2.016(4)	1.993(3)	1.99(2)	1.88(2)	1.93(2)	2.011(5)	1.994(4)[c]	1.998(6)
Ir–C	2.003(4)	2.007(4)	2.002(3)	2.01(2)	1.96(2)	2.006(9)	2.014(5)	1.995(5)[d]	1.984(6)
Ir–$N_{C\^N}$	2.043(3)	2.046(3)	2.041(3)	2.04(2)	2.05(2)	2.06(1)	2.049(4)	2.026(4)	2.055(5)
Ir–$N_{C\^N}$	2.044(3)	2.048(3)	2.042(3)	2.07(2)	2.05(2)	2.044(9)	2.052(4)	2.045(4)	2.060(5)
Ir–$N_{N\^N}$	2.128(3)	2.135(3)	2.113(3)	2.14(2)	2.14(2)	2.127(7)	2.124(4)		
Ir–$N_{N\^N}$	2.133(3)	2.136(4)	2.129(3)	2.00(2)	2.10(2)	2.128(8)	2.140(4)		
Ir–N_{MeCN}								2.112(4)	
Ir–Cl								2.458(1)	2.457(1)
Ir–Cl									2.470(1)
Angles (°)									
C–Ir–C	87.3(2)	86.6(2)	88.5(1)	85.8(9)	82.2(8)	84.4(7)	86.7(2)	90.0(2)	91.5(2)
C–Ir–$N_{N\^N}$	172.1(1)	173.5(1)	175.7(1)	174.4(8)	177.4(8)	175.4(7)	176.3(2)		
C–Ir–$N_{N\^N}$	97.3(2)	97.2(1)	100.0(1)	100.1(9)	101.8(8)	99.6(7)	96.4(2)		
C–Ir–$N_{N\^N}$	175.3(1)	176.3(2)	170.6(1)	172.8(8)	175.4(8)	175.8(4)	176.3(2)		
C–Ir–$N_{N\^N}$	99.0(1)	99.7(2)	95.3(1)	97.9(8)	99.8(8)	99.5(4)	100.0(2)		
C–Ir–N_{MeCN}								178.1(2)	
C–Ir–Cl								90.8(1)	87.3(2)
C–Ir–Cl									174.0(2)
C–Ir–N_{MeCN}								89.6(2)	
C–Ir–Cl								178.2(1)	174.9(2)
C–Ir–Cl									91.6(2)
C–Ir–$N_{C\^N}$	79.9(2)	79.7(2)	80.0(1)	80.5(8)	81.3(6)	80.6(4)	79.5(2)	79.8(2)	80.1(2)
C–Ir–$N_{C\^N}$	97.1(2)	93.1(2)	96.5(1)	95.5(8)	95.1(7)	94.5(4)	95.7(2)	97.4(2)	95.5(2)
C–Ir–$N_{C\^N}$	97.6(1)	95.1(2)	96.2(1)	97.3(8)	92.1(7)	91.8(6)	96.1(2)	95.7(2)	95.8(2)
C–Ir–$N_{C\^N}$	79.3(1)	79.7(2)	79.6(1)	79.8(8)	80.2(6)	84.9(7)	80.1(2)	80.1(2)	80.3(2)
$N_{C\^N}$–Ir–$N_{C\^N}$	175.8(1)	171.4(1)	174.7(1)	175.3(7)	171.9(6)	174.3(3)	174.1(1)	175.0(1)	174.1(2)
$N_{C\^N}$–Ir–$N_{N\^N}$	94.5(1)	98.2(1)	97.5(1)	94.8(6)	97.1(6)	97.7(3)	96.4(1)		
$N_{C\^N}$–Ir–$N_{N\^N}$	84.4(1)	87.5(1)	89.4(1)	87.8(8)	86.8(7)	86.4(3)	86.8(1)		
$N_{C\^N}$–Ir–$N_{N\^N}$	88.8(1)	87.6(1)	86.2(1)	89.4(7)	90.7(6)	87.3(3)	87.9(1)		
$N_{C\^N}$–Ir–$N_{N\^N}$	99.0(1)	100.0(1)	95.2(1)	95.4(7)	97.0(7)	97.3(4)	98.1(1)		
$N_{N\^N}$–Ir–$N_{N\^N}$	76.5(1)	76.6(1)	76.5(1)	76.6(6)	76.2(6)	76.5(3)	77.0(1)		
$N_{C\^N}$–Ir–N_{MeCN}								98.1(2)	
$N_{C\^N}$–Ir–Cl								84.3(1)	88.9(1)
$N_{C\^N}$–Ir–Cl									94.5(2)
$N_{C\^N}$–Ir–N_{MeCN}								86.0(2)	
$N_{C\^N}$–Ir–Cl								98.6(1)	94.9(2)
$N_{C\^N}$–Ir–Cl									90.1(2)
N_{MeCN}–Ir–Cl								89.7(1)	
Cl–Ir–Cl									90.04(5)

[a] Data taken from ref. 45. [b] For the two independent complex cations in the asymmetric unit. [c] *trans* with respect to the Cl^- ligand. [d] *trans* with respect to the MeCN ligand.

showing Ir–N_{MeCN} distances similar to or slightly longer than that in **10P**. The Ir–C distances in **10P** are indistinguishable, revealing no variation in structural *trans* effect between MeCN and Cl^-, despite the quite different bonding properties of these two ligands. Comparing the geometric parameters for the 2,2′-C^N complex in **10P** with those of the related complexes in **1P–3P** shows that replacing the N^N ligand with MeCN and Cl^- causes only minor changes which are mostly insignificant. The same applies for replacing N^N with Cl^- in the 4,2′-C^N complexes in **7P** and **11P**.

Electrochemistry

The results of cyclic and differential pulse voltammetric measurements on the PF_6^- salts **1P–9P** recorded in acetonitrile are shown in Table 3. Cyclic voltammograms of **1P–3P** are shown in Fig. 4. All potentials are quoted in V with respect to the Ag–AgCl reference electrode.

Each compound shows an irreversible oxidation process in the region *ca.* 2.2–2.5 V, which might be formally assigned to an $Ir^{IV/III}$ couple. The relatively high potentials when compared with related complexes of ppy[6,11–13,33–39,42] are attributable to the presence of the electron-deficient pyridinium units. DFT calculations (see below) show that the C^N ligands contribute to the HOMO significantly. With a given bipyridinium isomer, the E_{pa} value increases in the order N^N = 4,4′-(^{t}Bu)$_2$bpy < bpy < 4,4′-$(CF_3)_2$bpy, showing a modest influence (130–190 mV) of the R substituents. As N^N is kept constant, the E_{pa} value increases in the order C^N = 2,2′- ≈ 4,2′- < 3,2′-, revealing that the complexes in which the quaternised N atom is located *para* to the Ir centre are the most difficult to oxidise (by 180–240 mV).

The reductive regions include multiple processes (Fig. 4). For the 2,2′-C^N complexes in **1P–3P**, four reversible waves are observed, corresponding with sequential one-electron

Table 3 Electrochemical data for complex salts **1P–9P** in acetonitrile[a]

	E or $E_{1/2}$, V *vs.* Ag–AgCl (ΔE_p, mV)				
Salt (isomer)[b]	$Ir^{IV/III}$	3+/2+	2+/1+	1+/0	0/1−
1P (2)	2.18[c]	−0.78 (60)	−0.94 (70)	−1.38 (70)	−1.65 (80)
2P (2)	2.29[c]	−0.72 (60)	−0.86 (70)	−1.03 (60)	−1.56 (90)
3P (2)	2.16[c]	−0.78 (60)	−0.94 (70)	−1.45 (70)	−1.65 (70)
4P (3)[d]	2.36[c]	−1.13[e]	−1.26 (60)	−1.52[e]	—
5P (3)[d]	2.53[c]	−0.72 (70)	−1.26[e]	−1.44[e]	−1.65 (br)
6P (3)[d]	2.34[c]	−1.18[e]	−1.36[e]	−1.56[e]	—
7P (4)	2.19[c]	−0.83 (70)	−0.99 (60)	−1.41 (70)	—
8P (4)	2.30[c]	−0.73 (70)	−0.90 (60)	−1.07 (70)	—
9P (4)	2.16[c]	−0.82 (80)	−0.98 (80)	−1.48 (80)	−1.76 (80)

[a] Solutions *ca.* 1.5×10^{-4} M in analyte and 0.1 M in $[N^nBu_4]PF_6$ at a 2 mm disc platinum working electrode with a scan rate of 100 mV s^{-1}. Ferrocene internal standard $E_{1/2}$ = 0.44 V, ΔE_p = 70–90 mV. [b] Denotes the position with respect to the quaternised N atom of the N-coordinated 2′-pyridyl ring. [c] E_{pa} for an irreversible oxidation process determined *via* differential pulse voltammetry: potential increment = 2 mV; amplitude = 50 mV; pulse width = 0.01 s. [d] Data taken from ref. 45. [e] E_{pc} for an irreversible reduction process.

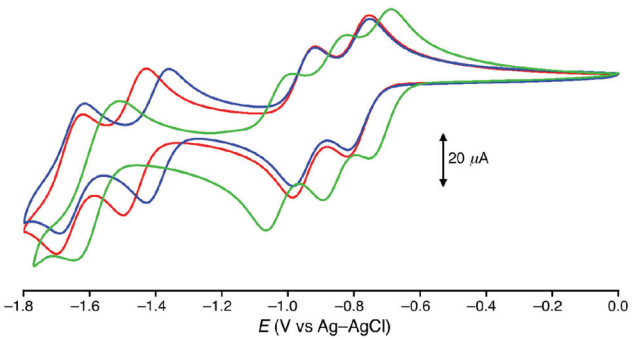

Fig. 4 Cyclic voltammograms depicting the reduction processes of complex salts **1P** (blue), **2P** (green) and **3P** (red) recorded at 100 mV s^{-1} in acetonitrile 0.1 M in $[N^nBu_4]PF_6$ at 295 K.

reductions to give a monoanionic final product. The $E_{1/2}$ values are similar for the complexes of bpy (**1**) and 4,4′-(^{t}Bu)$_2$bpy (**3**), while those for the complex of 4,4′-$(CF_3)_2$bpy (**2**) are lower by 60–420 mV, because the electron-withdrawing influence of the $-CF_3$ groups facilitates reduction. Similar behaviour is shown by the 4,2′-C^N complexes in **7P–9P**, except that **7** and **8** display only three waves instead of four. For both 2,2′- and 4,2′-C^N series, the 1+/0 $E_{1/2}$ value shows the largest dependence on R, suggesting that this third reduction is localised on the N^N ligand. Therefore, the first and second reductions may be assigned to the C^N ligands. In contrast, the reductive behaviour of the 3,2′-C^N complexes in **4P–6P** is much less well-defined, with most of the processes being irreversible. Also, sharp anodic return peaks are observed for **1** and **3**, indicative of adsorption onto the electrode surface. The nature of these data preclude the discernment of any further trends.

Electronic absorption spectroscopy

The absorption spectral data for the PF_6^- salts of the new complexes **1–3** and **7–9** recorded in acetonitrile are shown in Table 4, together with those for **4–6**.[45] Corresponding data for the Cl^- salts in water are collected in Table S2,† and spectra of **1P–4P** and **7P** are shown in Fig. 5.

All of complexes **1–9** show intense bands below 320 nm which are assigned to $\pi \rightarrow \pi^*$ and high energy MLCT transitions involving both the C^N and N^N ligands. Weaker bands are observed also, with tails extending up to *ca.* 480 nm in some cases. The lowest energy (LE) band is clearly blue-shifted in the 3,2′-C^N complexes **4–6** (λ_{max} for shoulders ≈ 350–360 nm) when compared with the new complexes **1–3** and **7–9** (λ_{max} for shoulders ≈ 425–445 nm) (Fig. 5a). DFT shows that this band in **4–6** has ^{1}MLCT character with some ^{1}ML′CT and also ^{1}LL′CT contributions for **4** and **5** (L = C^N; L′ = N^N).[45] The slight shifts (*ca.* 0.1 eV) when R changes (Fig. 5b) are consistent with the largely ^{1}MLCT assignment. The observed blue-shifts when varying the structure of the C^N ligands are attributable to destabilisation of their π^* orbitals because the *para*-position of the quaternised N increases its neutral carbene character. Therefore, the energy gap of the MLCT transition increases in **4–6** with respect to their isomeric counterparts **1–3** and **7–9**. The absorption spectra are almost unaffected by changing the counter-anions and solvent (Tables 4 and S2†).

Luminescence properties

The emission spectral data for the PF_6^- and Cl^- salts of the new complexes **1–3** and **7–9** recorded in deoxygenated and oxygenated acetonitrile or water are shown in Table 5, together with those for **4–6**.[45] Spectra of **1P**, **4P** and **7P** are shown in Fig. 6, while those of the other compounds are in the ESI (Fig. S1 and S2†). Changing the counter-anion and solvent has only slight effects on the excitation profiles that remain constant in all cases while monitoring at all the emission maxima.

All of the spectra are structured, especially for complexes **4–6**,[45] indicating significant ligand contributions to the luminescence. The profiles and emission energies of **1–3** and **7–9** are similar and red-shifted when compared to **4–6** (Fig. 6, S1 and S2†). The importance of the position of the quaternised

Table 4 UV–vis absorption data for complex salts **1P–9P** in acetonitrile[a]

Salt (isomer)[b]	λ_{max}, nm (ε, 10^3 M^{-1} cm^{-1})	E_{max} (eV)	Assignment
1P (2)	212sh (53.1)	5.85	$\pi \rightarrow \pi^*$
	257 (34.4)	4.82	$\pi \rightarrow \pi^*$
	297 (33.3)	4.18	$\pi \rightarrow \pi^*$
	354 (9.4)	3.50	$d \rightarrow \pi^*$
	437sh (2.8)	2.84	$d \rightarrow \pi^*$
2P (2)	212 (48.2)	5.85	$\pi \rightarrow \pi^*$
	263 (32.3)	4.71	$\pi \rightarrow \pi^*$
	298 (29.7)	4.16	$\pi \rightarrow \pi^*$
	350sh (10.2)	3.54	$d \rightarrow \pi^*$
	426sh (3.4)	2.91	$d \rightarrow \pi^*$
3P (2)	213 (60.4)	5.82	$\pi \rightarrow \pi^*$
	258 (35.2)	4.81	$\pi \rightarrow \pi^*$
	299 (34.0)	4.15	$\pi \rightarrow \pi^*$
	312sh (28.9)	3.97	$d \rightarrow \pi^*$
	355 (9.1)	3.49	$d \rightarrow \pi^*$
	445sh (2.3)	2.79	$d \rightarrow \pi^*$
4P (3)[c]	237 (54.3)	5.23	$\pi \rightarrow \pi^*$
	255sh (48.5)	4.86	$\pi \rightarrow \pi^*$
	302 (25.9)	4.11	$\pi \rightarrow \pi^*$
	313 (24.5)	3.96	$d \rightarrow \pi^*$
	352sh (5.3)	3.52	$d \rightarrow \pi^*$
5P (3)[c]	237 (52.7)	5.23	$\pi \rightarrow \pi^*$
	259 (52.1)	4.79	$\pi \rightarrow \pi^*$
	308 (25.2)	4.03	$\pi \rightarrow \pi^*$
	317 (24.3)	3.91	$d \rightarrow \pi^*$
	350sh (5.8)	3.54	$d \rightarrow \pi^*$
6P (3)[c]	237 (58.0)	5.23	$\pi \rightarrow \pi^*$
	260 (49.9)	4.77	$\pi \rightarrow \pi^*$
	300 (25.4)	4.13	$\pi \rightarrow \pi^*$
	312 (25.9)	3.97	$d \rightarrow \pi^*$
	355sh (5.5)	3.49	$d \rightarrow \pi^*$
7P (4)	254 (44.8)	4.88	$\pi \rightarrow \pi^*$
	280sh (32.2)	4.43	$\pi \rightarrow \pi^*$
	307 (28.1)	4.04	$\pi \rightarrow \pi^*$
	357 (6.8)	3.47	$d \rightarrow \pi^*$
	392sh (3.8)	3.16	$d \rightarrow \pi^*$
	435sh (1.9)	2.85	$d \rightarrow \pi^*$
8P (4)	252 (46.2)	4.92	$\pi \rightarrow \pi^*$
	295 (32.7)	4.20	$\pi \rightarrow \pi^*$
	307 (31.7)	4.04	$\pi \rightarrow \pi^*$
	350sh (7.8)	3.54	$d \rightarrow \pi^*$
	389 (5.0)	3.19	$d \rightarrow \pi^*$
	425sh (2.6)	2.92	$d \rightarrow \pi^*$
9P (4)	234 (44.6)	5.30	$\pi \rightarrow \pi^*$
	256 (50.1)	4.84	$\pi \rightarrow \pi^*$
	299 (31.7)	4.15	$\pi \rightarrow \pi^*$
	309 (30.0)	4.01	$\pi \rightarrow \pi^*$
	358 (7.2)	3.46	$d \rightarrow \pi^*$
	394sh (3.8)	3.15	$d \rightarrow \pi^*$
	440sh (1.9)	2.82	$d \rightarrow \pi^*$

[a] Solutions *ca.* 1×10^{-5}–2×10^{-4} M; ε values are the averages from measurements made at three or more different concentrations (with ε showing no significant variation). [b] Denotes the position with respect to the quaternised N atom of the N-coordinated 2′-pyridyl ring. [c] Data taken from ref. 45.

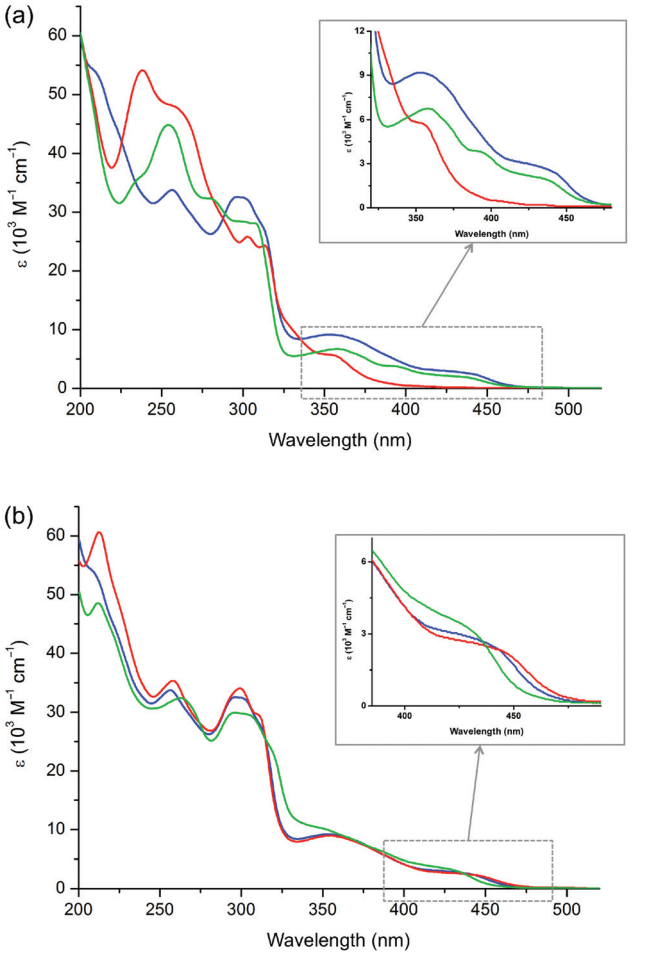

Fig. 5 UV–vis absorption spectra of complex salts **1P** (blue), **4P** (red) and **7P** (green) (a); **1P** (blue), **2P** (green) and **3P** (red) (b); recorded in acetonitrile at 295 K.

N is evident; when it is located *meta* to the cyclometalating C atom, green emission is observed (λ_{max} = 508–530 nm), but when it is positioned *para* to the C, blue or blue-green emission arises (λ_{max} = 468–494 nm). This difference is attributable to the almost carbene-like character and consequent relative orbital energies in **4–6**. Various other types of Ir complexes emit in the green region, *e.g.* $[Ir^{III}(ppy\text{-}PBu_3)_3][PF_6]_2$ [ppy-PBu_3 = cyclometalated 2-(5-tri-*n*-butylphosphoniumphenyl)pyridine][69] and monocationic complexes of 4,4′-(^{t}Bu)$_2$bpy with –SF_5 substituents on the C^N ligands.[70]

The influence of the R substituents in the 2,2′-C^N (**1–3**) and 4,2′-C^N (**7–9**) complexes is small. The emission energies follow the expected trend R = ^{t}Bu < H < CF_3, but with a difference of only *ca.* 0.05 eV between the extremes (Table 5). This effect can be attributed to the stabilisation of the metal orbitals caused by placing electron-withdrawing groups on the ancillary ligand. These results suggest that in all of these new complexes the emission has a mainly ^{3}LC character involving the C^N ligand with some ^{3}MLCT contribution. By contrast, for the 3,2′-C^N complexes, such a situation pertains for **4** and **6**, but **5** behaves differently and gives N^N-based emission.[45] Therefore, in that series the emission energy is decreased (and the bands red-shifted) for the –CF_3 derivative with respect to the other complexes.

When keeping N^N constant, the quantum yields (Φ) of **1–3** and **7–9** are generally similar to, or a little larger than those of

Table 5 Luminescence data for complex salts **1P–9P** and **1C–9C**[a]

Salt (isomer)[b]	λ_{em} [c] (nm)	τ^d (μs)		ϕ^d (%)	
		deox	ox	deox	ox
1P (2)	526, 550	1.3	0.9	33	16
1C (2)	527, 555	3.9	2.3	59	29
2P (2)	519, 540	1.4	0.8	34	15
2C (2)	518, 545	4.1	1.8	44	20
3P (2)	530, 556	2.0	0.9	38	23
3C (2)	530, 558	3.9	2.1	43	25
4P (3)[e]	444, 474$_{max}$, 504, 548	3.5	1.2	24	4.7
4C (3)[e]	442, 470$_{max}$, 504, 547	12.1	3.9	27	9.6
5P (3)[e]	466, 494$_{max}$, 525, 574	3.8	1.5	43	16
5C (3)[e]	462, 494$_{max}$, 529, 575	4.3	2.5	42	24
6P (3)[e]	440, 470$_{max}$, 502, 546	3.8	1.2	43	10
6C (3)[e]	440, 468$_{max}$, 500, 547	9.5	2.9	45	14
7P (4)	520, 548	2.0	1.2	30	15
7C (4)	518, 549, 609	3.9	2.2	60	32
8P (4)	510, 540	2.9	1.4	44	22
8C (4)	508, 540, 592	4.7	2.7	56	33
9P (4)	522, 555	2.3	1.0	44	18
9C (4)	522, 553, 613	3.4	1.9	52	27

[a] Solutions 5×10^{-5} M in acetonitrile for PF_6^- salts, water for Cl^- salts. [b] Denotes the position with respect to the quaternised N atom of the N-coordinated 2′-pyridyl ring. [c] With excitation over the range 350–440 nm for **1–3** and **7–9**, and 315–400 nm for **4–6**. deox = deoxygenated; ox = oxygenated. [d] Estimated experimental errors ±10%. [e] Data taken from ref. 45.

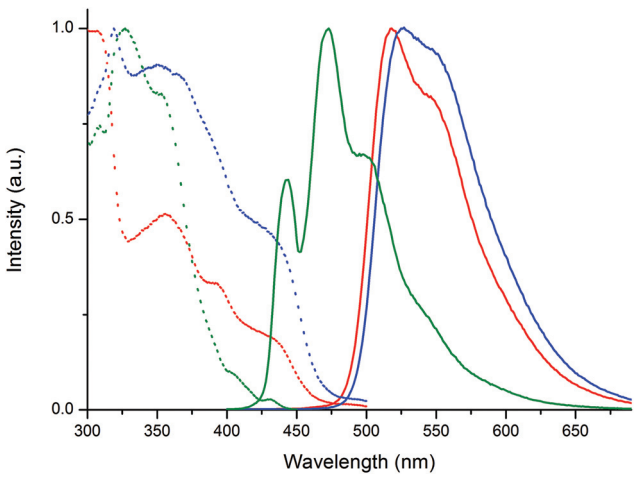

Fig. 6 Emission (full lines; excitation at 350 nm) and excitation (dashed lines) spectra of the bpy-containing complex salts **1P** (blue), **4P** (green) and **7P** (red) recorded in acetonitrile at 295 K.

4–6 (Table 5), showing that moving the quaternised N to a *meta*-position with respect to the cyclometalating C does not facilitate non-radiative decay. In contrast to the almost invariant emission energies, τ always increases and Φ increases in most instances (sometimes markedly) on moving from a PF_6^- salt in acetonitrile to its Cl^- analogue in water. In all cases, both τ and Φ increase substantially on deoxygenation, consistent with emission originating from triplet excited states.

Theoretical calculations

DFT and TD-DFT calculations have been carried out on the complexes **1–3** and **7** by using the M06 functional with the Def2-QZVP basis set on Ir and Def2-SVP on all other atoms, as used for **4–6** previously.[45]

The optimised structures in the ground state agree well with the data obtained from X-ray crystallography (see the ESI, Table S3†). Selected MOs are depicted in Fig. S3–S6,† and the orbital compositions are shown in Table S4.† The frontier orbitals HOMO−2 to LUMO+2 are essentially invariant within the cations **1–3** and **7**. The HOMO−1 and HOMO−2 are mainly centered on the Ir atom (67–72%) with some contribution from the C^N ligand (16–22%), while the HOMO has almost the same contribution from both fragments (Ir 47–55%; C^N 43–51%). The LUMO and LUMO+1 are based on C^N almost completely (96–98%), while the LUMO+2 is located on N^N (95–97%).

The $S_0 \rightarrow S_1$ transition energies calculated in acetonitrile and the corresponding major orbital contributions are presented in Table S5 (ESI†). The simulated absorption spectra for complexes **1–3** agree well with those measured (Fig. 7). The calculated wavelengths of the LE transitions 421 (**1**), 412 (**2**), 424 (**3**) and 416 nm (**7**) are slightly blue shifted with respect to the experimental λ_{max} values (437 (**1**), 426 (**2**), 445 (**3**) and 435 nm (**7**); Table 4). In all complexes, this transition has almost pure HOMO → LUMO character (92–95%). Therefore, the LE bands can be assigned to a mixture of ^{1}LC and ^{1}MLCT (L = C^N). The observed modest dependence of the LE transition on the R substituents is reproduced by the calculations on **1–3**, *i.e.* ΔE increases in the order R = ^{t}Bu < H < CF_3. Comparisons with the data obtained for **4–6**[45] show that the level of theory applied also predicts the red-shifts of the LE band observed on moving from the 3,2′-C^N complexes to their 2,2′-C^N counterparts **1–3** (and for **4** → **7**); the calculated λ values are 347 (**4**), 342 (**5**) and 348 nm (**6**).

For **1–3** and **7**, the first computed transition involving mainly the N^N ligand (*i.e.* a dominant component to LUMO+2; in all cases HOMO−2 → LUMO+2 ^{1}MLCT) lies to markedly higher energy when compared with the LE transition. The electronic influence of the R substituents is manifested in the predicted energies. The transition is at 3.90 eV (318 nm) for **1**, 3.99 eV (311 nm) for **3** and 3.87 eV (320 nm) for **7**, but 3.69 eV (336 nm) for **2** due to the stabilisation of the LUMO+2 by the $-CF_3$ groups.

The nature of the luminescence was addressed by optimising the first triplet excited states T_1 of **1–3** and **7**. The computed geometric parameters of these states are similar to those found for the corresponding ground states S_0 (Table S3, ESI†). The lowest energy emissions calculated in acetonitrile as $\Delta E(T_1 - S_0)$ at 531 (**1**), 527 (**2**), 538 (**3**) and 521 nm (**7**) are close to the experimental values (526 (**1**), 519 (**2**), 530 (**3**) and 520 nm (**7**); Table 5). Also, the calculations reproduce the experimental trend in the emission wavelengths (λ_{em} **2** < **1** < **3**). The spin densities for the T_1 state for all complexes (Fig. 8) are located mainly on one C^N ligand, together with the Ir atom to

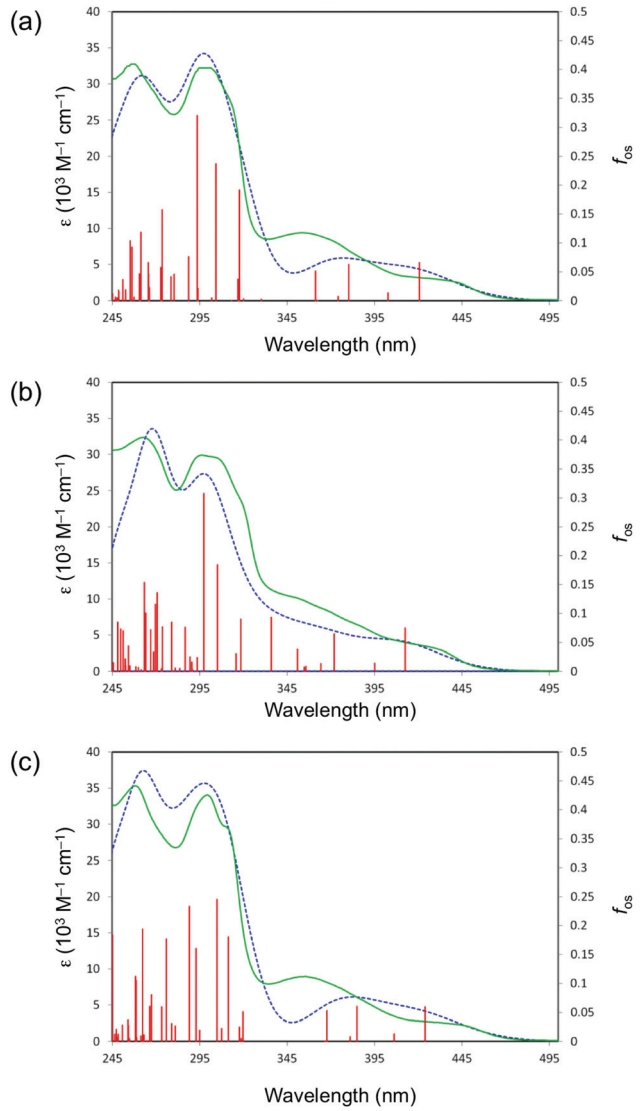

Fig. 7 M06/Def2-QZVP/Def2-SVP-calculated (blue) UV–vis spectra of (a) **1**, (b) **2** and (c) **3**, and the corresponding experimental data (green) for the PF_6^- salts in acetonitrile. The ε-axes refer to the experimental data only and the vertical axes of the calculated data are scaled to match the main experimental absorptions. The oscillator strength axes refer to the individual calculated transitions (red).

a lesser extent. Therefore, the emissions can be assigned as ^{3}LC involving the cyclometalating ligand with some ^{3}MLCT contribution. These results are similar to those obtained for complexes **4** and **6**,[45] showing that the only complex of the nine studied with a different nature of the emission is **5**. In that case, the $-CF_3$ substituents stabilise the ^{3}L′C state, causing efficient inter-ligand energy transfer from the C^N to the emitting N^N fragment. In complex **2**, the stabilisation due to the $-CF_3$ groups is insufficient to bring the energy of the ^{3}L′C below the ^{3}LC state.

Conclusions

We have synthesised and characterised a series of new Ir^{III} complexes by using three different isomers of 1-methyl-(2′-pyridyl)pyridinium to generate cyclometalating ligands C^N. Because the latter are charge-neutral, adding an α-diimine ancillary ligand N^N affords species with a 3+ charge and unusually high solubility in water when isolated as Cl^- salts. Such enhanced aqueous solubility increases the prospects for applications in bioimaging. The complexes are characterised fully as both their PF_6^- and Cl^- salts, and in four cases, their structures are confirmed by single-crystal X-ray crystallography. Electrochemistry reveals for each complex an irreversible oxidation of the $\{Ir^{III}(C^N)_2\}^{3+}$ unit and multiple ligand-based one-electron reductions. The reductive behaviour is much better defined for the new 2,2′-C^N and 4,2′-C^N complexes when compared with their 3,2′-C^N counterparts, with up to four reversible waves being observed. Within each series, the redox potentials are affected significantly by varying the R substituents on the N^N ligand. All of the complex salts appear yellow coloured and their UV–vis absorption spectra show low energy bands in the region *ca.* 350–450 nm. DFT and TD-DFT calculations using the M06 functional confirm that these are attributable to ^{1}MLCT transitions with some ^{1}LC, ^{1}ML′CT and also ^{1}LL′CT contributions. Changing the N^N ligand while keeping C^N constant affects the absorption spectra only slightly. The observed red-shifts of the low energy bands for the 2,2′-C^N and 4,2′-C^N complexes with respect their 3,2′-C^N

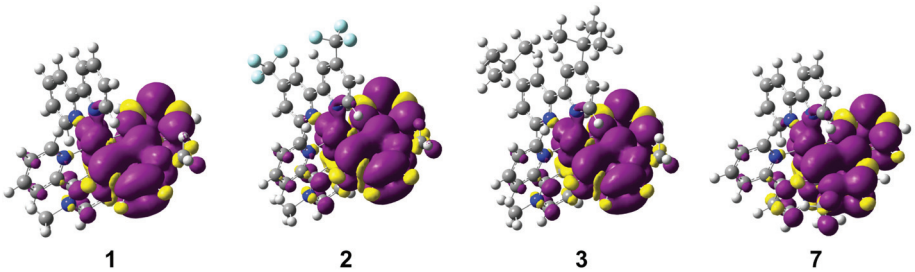

Fig. 8 M06/Def2-QZVP-SVP-calculated spin density plots for the T_1 state of the complexes **1**, **2**, **3** and **7**. In each case, the N^N ligand is pointing upwards.

analogues are reproduced theoretically. In contrast to the 3,2′-C^N complexes that show intense blue or blue-green emission, the new isomeric species are all green emitters. The emission is shown by DFT to originate from ^{3}LC excited states involving the cyclometalating ligand with some ^{3}MLCT contribution. Therefore, changing the N^N ligand has only a minor influence on the luminescence. Neither the absorption nor emission spectra show more than slight solvent dependence. In terms of future prospects, there is great scope for modifying the optical properties of these highly charged complexes, for example by changing the substituent on the quaternised N atom and/or attaching other groups to either the C^N or N^N ligands.

Acknowledgements

We thank the EPSRC for support (grant EP/J018635/1), and the BBSRC for a PhD studentship (M. K. P.). N. S. S. is supported by an EPSRC Established Career Fellowship (grant EP/J020192/1) and was funded by a Royal Society Wolfson Merit Award. We thank Dr Sarah L. Heath for solving the X-ray crystal structure of **7P**·MeCN·Et_2O, and Dr Louise S. Natrajan and Michael B. Andrews for assistance with the luminescence measurements.

References

1 M. S. Lowry and S. Bernhard, *Chem. – Eur. J.*, 2006, **12**, 7970–7977.
2 L. Flamigni, A. Barbieri, C. Sabatini, B. Ventura and F. Barigelletti, *Top. Curr. Chem.*, 2007, **281**, 143–203.
3 J. A. G. Williams, A. J. Wilkinson and V. L. Whittle, *Dalton Trans.*, 2008, 2081–2099.
4 Y. Chi and P.-T. Chou, *Chem. Soc. Rev.*, 2010, **39**, 638–655.
5 Y.-M. You and W.-W. Nam, *Chem. Soc. Rev.*, 2012, **41**, 7061–7084.
6 S. Ladouceur and E. Zysman-Colman, *Eur. J. Inorg. Chem.*, 2013, 2985–3007.
7 K. P. S. Zanoni, R. L. Coppo, R. C. Amaral and N. Y. Murakami Iha, *Dalton Trans.*, 2015, **44**, 14559–14573.
8 M. A. Baldo, M. E. Thompson and S. R. Forest, *Nature*, 2000, **403**, 750–753.
9 Y. You and S. Y. Park, *J. Am. Chem. Soc.*, 2005, **127**, 12438–12439.
10 C.-L. Ho, H. Li and W.-Y. Wong, *J. Organomet. Chem.*, 2014, **751**, 261–285.
11 J. D. Slinker, A. A. Gorodetsky, M. S. Lowry, J.-J. Wang, S. Parker, R. Rohl, S. Bernhard and G. G. Malliaras, *J. Am. Chem. Soc.*, 2004, **126**, 2763–2767.
12 M. Mydlak, C. Bizzarri, D. Hartmann, W. Sarfert, G. Schmid and L. De Cola, *Adv. Funct. Mater.*, 2010, **20**, 1812–1820.
13 T. Hu, L. He, L. Duan and Y. Qiu, *J. Mater. Chem.*, 2012, **22**, 4206–4215.
14 K. K.-W. Lo, M.-W. Louie and K. Y. Zhang, *Coord. Chem. Rev.*, 2010, **254**, 2603–2622.
15 Q. Zhao, C. Huang and F. Li, *Chem. Soc. Rev.*, 2011, **40**, 2508–2524.
16 E. Baggaley, J. A. Weinstein and J. A. G. Williams, *Coord. Chem. Rev.*, 2012, **256**, 1762–1785.
17 Y. You, S. Cho and W. Nam, *Inorg. Chem.*, 2014, **53**, 1804–1815.
18 K. K.-W. Lo and S. P.-Y. Li, *RSC Adv.*, 2014, **4**, 10560–10585.
19 S. Stimpson, D. R. Jenkinson, A. Sadler, M. Latham, A. Wragg, A. J. H. M. Meijer and J. A. Thomas, *Angew. Chem., Int. Ed.*, 2015, **54**, 3000–3003.
20 K. Y. Zhang, S.-J. Liu, Q. Zhao, F. Li and W. Huang, *Struct. Bonding*, 2015, **165**, 131–180.
21 S. J. Lee, K.-M. Park, K. Yang and Y. Kang, *Inorg. Chem.*, 2009, **48**, 1030–1037.
22 C.-H. Yang, M. Mauro, F. Polo, S. Watanabe, I. Muenster, R. Fröhlich and L. De Cola, *Chem. Mater.*, 2012, **24**, 3684–3695.
23 C.-H. Chang, Z.-J. Wu, C.-H. Chiu, Y.-H. Liang, Y.-S. Tsai, J.-L. Liao, Y. Chi, H.-Y. Hsieh, T.-Y. Kuo, G.-H. Lee, H.-A. Pan, P.-T. Chou, J.-S. Lin and M.-R. Tseng, *ACS Appl. Mater. Interfaces*, 2013, **5**, 7341–7351.
24 Y. Kang, Y.-L. Chang, J.-S. Lu, S.-B. Ko, Y. Rao, M. Varlan, Z.-H. Lu and S. Wang, *J. Mater. Chem. C*, 2013, **1**, 441–450.
25 F. Kessler, Y. Watanabe, H. Sasabe, H. Katagiri, M. K. Nazeeruddin, M. Grätzel and J. Kido, *J. Mater. Chem. C*, 2013, **1**, 1070–1075.
26 J. Frey, B. F. E. Curchod, R. Scopelliti, I. Tavernelli, U. Rothlisberger, M. K. Nazeeruddin and E. Baranoff, *Dalton Trans.*, 2014, **43**, 5667–5679.
27 N. Darmawan, C.-H. Yang, M. Mauro, R. Fröhlich, L. De Cola, C.-H. Chang, Z.-J. Wu and C.-W. Tai, *J. Mater. Chem. C*, 2014, **2**, 2569–2582.
28 J. Lee, H. Oh, J. Kim, K.-M. Park, K. S. Yook, J. Y. Lee and Y. Kang, *J. Mater. Chem. C*, 2014, **2**, 6040–6047.
29 J.-B. Kim, S.-H. Han, K. Yang, S.-K. Kwon, J.-J. Kim and Y.-H. Kim, *Chem. Commun.*, 2015, **51**, 58–61.
30 K. P. S. Zanoni, A. Ito and N. Y. Murakami Iha, *New J. Chem.*, 2015, **39**, 6367–6376.
31 J. Feldman, G. D. Vo, C. D. McLaren, T. C. Gehret, K.-H. Park, J. S. Meth, W. J. Marshall, J. Buriak, L. M. Bryman, K. D. Dobbs, T. H. Scholz and S. G. Zane, *Organometallics*, 2015, **34**, 3665–3669.
32 T. Duan, T.-K. Chang, Y. Chi, J.-Y. Wang, Z.-N. Chen, W.-Y. Hung, C.-H. Chen and G.-H. Lee, *Dalton Trans.*, 2015, **44**, 14613–14624.
33 M. S. Lowry, J. I. Goldsmith, J. D. Slinker, R. Rohl, R. A. Pascal Jr., G. G. Malliaras and S. Bernhard, *Chem. Mater.*, 2005, **17**, 5712–5719.
34 S. Ladouceur, D. Fortin and E. Zysman-Colman, *Inorg. Chem.*, 2010, **49**, 5625–5641.
35 S. B. Meier, W. Sarfert, J. M. Junquera-Hernández, M. Delgado, D. Tordera, E. Ortí, H. J. Bolink, F. Kessler, R. Scopelliti, M. Grätzel, M. K. Nazeeruddin and E. Baranoff, *J. Mater. Chem. C*, 2013, **1**, 58–68.

36 E. C. Constable, C. E. Housecroft, P. Kopecky, C. J. Martin, I. A. Wright, J. A. Zampese, H. J. Bolink and A. Pertegas, *Dalton Trans.*, 2013, **42**, 8086–8103.
37 S. Evariste, M. Sandroni, T. W. Rees, C. Roldán-Carmona, L. Gil-Escrig, H. J. Bolink, E. Baranoff and E. Zysman-Colman, *J. Mater. Chem. C*, 2014, **2**, 5793–5804.
38 A. F. Henwood, S. Evariste, A. M. Z. Slawin and E. Zysman-Colman, *Faraday Discuss.*, 2014, **174**, 165–182.
39 G. E. Schneider, A. Pertegás, E. C. Constable, C. E. Housecroft, N. Hostettler, C. D. Morris, J. A. Zampese, H. J. Bolink, J. M. Junquera-Hernández, E. Ortí and M. Sessolo, *J. Mater. Chem. C*, 2014, **2**, 7047–7055.
40 K. Hasan, A. K. Pal, T. Auvray, E. Zysman-Colman and G. S. Hanan, *Chem. Commun.*, 2015, **51**, 14060–14063.
41 S. Lamansky, P. Djurovich, D. Murphy, F. Abdel-Razzaq, H.-E. Lee, C. Adachi, P. E. Burrows, S. R. Forrest and M. E. Thompson, *J. Am. Chem. Soc.*, 2001, **123**, 4304–4312.
42 K. K.-W. Lo, K. Y. Zhang, C.-K. Chung and K. Y. Kwok, *Chem. – Eur. J.*, 2007, **13**, 7110–7120.
43 C. Dragonetti, S. Righetto, D. Roberto, R. Ugo, A. Valore, F. Demartin, F. De Angelis, A. Sgamellotti and S. Fantacci, *Inorg. Chim. Acta*, 2008, **361**, 4070–4076.
44 M. S. Lowry, W. R. Hudson, R. A. Pascal Jr. and S. Bernhard, *J. Am. Chem. Soc.*, 2004, **126**, 14129–14135.
45 B. J. Coe, M. Helliwell, S. Sánchez, M. K. Peers and N. S. Scrutton, *Dalton Trans.*, 2015, **44**, 15420–15423.
46 G. Song, Y. Zhang, Y. Su, W. Deng, K. Han and X. Li, *Organometallics*, 2008, **27**, 6193–6201.
47 (*a*) S. Dholakia, R. D. Gillard and F. L. Wimmer, *Inorg. Chim. Acta*, 1983, **69**, 179–181; (*b*) F. L. Wimmer and S. Wimmer, *Polyhedron*, 1985, **4**, 1665–1666; (*c*) F. L. Wimmer and S. Wimmer, *Transition Met. Chem.*, 1985, **10**, 238–240; (*d*) P. Castan, F. Dahan, S. Wimmer and F. L. Wimmer, *J. Chem. Soc., Dalton Trans.*, 1990, 2971–2977; (*e*) P. S. Braterman, J.-I. Song, F. L. Wimmer and S. Wimmer, *Inorg. Chim. Acta*, 1991, **189**, 7–9; (*f*) P. Castan, J. Jaud, S. Wimmer and F. L. Wimmer, *J. Chem. Soc., Dalton Trans.*, 1991, 1155–1158; (*g*) F. L. Wimmer, S. Wimmer and P. Castan, *J. Organomet. Chem.*, 1992, **424**, 99–104; (*h*) M. R. Snow and E. R. T. Tiekink, *Z. Kristallogr.*, 1992, **198**, 148–150; (*i*) P. S. Braterman, J.-I. Song, F. M. Wimmer, S. Wimmer, W. Kaim, A. Klein and R. D. Peacock, *Inorg. Chem.*, 1992, **31**, 5084–5088; (*j*) P. Castan, B. Labiad, D. Villemin, F. L. Wimmer and S. Wimmer, *J. Organomet. Chem.*, 1994, **479**, 153–157; (*k*) S. Wimmer and F. L. Wimmer, *J. Chem. Soc., Dalton Trans.*, 1994, 879–884; (*l*) L. Yang, F. L. Wimmer, S. Wimmer, J. Zhao and P. S. Braterman, *J. Organomet. Chem.*, 1996, **525**, 1–8.
48 T. Koizumi, T. Tomon and K. Tanaka, *J. Organomet. Chem.*, 2005, **690**, 1258–1264.
49 (*a*) Y. Ma, S.-J. Liu, H.-R. Yang, Y.-Q. Wu, C.-J. Yang, X.-M. Liu, Q. Zhao, H.-Z. Wu, J.-C. Liang, F.-Y. Li and W. Huang, *J. Mater. Chem.*, 2011, **21**, 18974–18982; (*b*) Y.-Y. Zhou, J.-L. Jia, W.-F. Li, H. Fei and M. Zhou, *Chem. Commun.*, 2013, **49**, 3230–3232; (*c*) S.-J. Liu, H. Liang, K. Y. Zhang, Q. Zhao, X.-B. Zhou, W.-J. Xu and W. Huang, *Chem. Commun.*, 2015, **51**, 7943–7946.
50 M. C. Burla, R. Caliandro, M. Camalli, B. Carrozzini, G. L. Cascarano, L. De Caro, C. Giacovazzo, G. Polidori and R. Spagna, *J. Appl. Crystallogr.*, 2005, **32**, 381–388.
51 G. M. Sheldrick, *Acta Crystallogr., Sect. A: Fundam. Crystallogr.*, 1990, **46**, 467.
52 G. M. Sheldrick, *Acta Crystallogr., Sect. C: Struct. Chem.*, 2015, **71**, 3–8.
53 M. J. Frisch, G. W. Trucks, H. B. Schlegel, G. E. Scuseria, M. A. Robb, J. R. Cheeseman, G. Scalmani, V. Barone, B. Mennucci, G. A. Petersson, H. Nakatsuji, M. Caricato, X. Li, H. P. Hratchian, A. F. Izmaylov, J. Bloino, G. Zheng, J. L. Sonnenberg, M. Hada, M. Ehara, K. Toyota, R. Fukuda, J. Hasegawa, M. Ishida, T. Nakajima, Y. Honda, O. Kitao, H. Nakai, T. Vreven, J. J. A. Montgomery, J. E. Peralta, F. Ogliaro, M. Bearpark, J. J. Heyd, E. Brothers, K. N. Kudin, V. N. Staroverov, T. Keith, R. Kobayashi, J. Normand, K. Raghavachari, J. C. A. Rendell, J. C. Burant, S. S. Iyengar, J. Tomasi, M. Cossi, N. Rega, J. M. Millam, M. Klene, J. E. Knox, J. B. Cross, V. Bakken, C. Adamo, J. Jaramillo, R. Gomperts, R. E. Stratmann, O. Yazyev, A. J. Austin, R. Cammi, C. Pomelli, J. W. Ochterski, R. L. Martin, K. Morokuma, V. G. Zakrzewski, G. A. Voth, P. Salvador, J. J. Dannenberg, S. Dapprich, A. D. Daniels, O. Farkas, J. B. Foresman, J. V. Ortiz, J. Cioslowski and D. J. Fox, *GAUSSIAN 09 (Revision B.01)*, Gaussian, Inc., Wallingford CT, 2010.
54 Y. Zhao and D. Truhlar, *Theor. Chem. Acc.*, 2008, **120**, 215–241.
55 F. Weigend, F. Furche and R. Ahlrichs, *J. Chem. Phys.*, 2003, **119**, 12753–12762.
56 D. Andrae, U. Häußermann, M. Dolg, H. Stoll and H. Preuß, *Theor. Chim. Acta*, 1990, **77**, 123–141.
57 F. Weigend and R. Ahlrichs, *Phys. Chem. Chem. Phys.*, 2005, **7**, 3297–3305.
58 V. Barone and M. Cossi, *J. Phys. Chem. A*, 1998, **102**, 1995–2001.
59 M. Cossi, N. Rega, G. Scalmani and V. Barone, *J. Comput. Chem.*, 2003, **24**, 669–681.
60 N. M. O'Boyle, A. L. Tenderholt and K. M. Langner, *J. Comput. Chem.*, 2008, **29**, 839–845.
61 T. Sajoto, P. I. Djurovich, A. Tamayo, M. Yousufuddin, R. Bau and M. E. Thompson, *Inorg. Chem.*, 2005, **44**, 7992–8003.
62 K.-Y. Lu, H.-H. Chou, C.-H. Hsieh, Y.-H. O. Yang, H.-R. Tsai, H.-Y. Tsai, L.-C. Hsu, C.-Y. Chen, I.-C. Chen and C.-H. Cheng, *Adv. Mater.*, 2011, **23**, 4933–4937.
63 B. D. Stringer, L. M. Quan, P. J. Barnard, D. J. D. Wilson and C. F. Hogan, *Organometallics*, 2014, **33**, 4860–4872.
64 F. Monti, M. G. I. La Placa, N. Armaroli, R. Scopelliti, M. Grätzel, M. K. Nazeeruddin and F. Kessler, *Inorg. Chem.*, 2015, **54**, 3031–3042.
65 N. Zhao, Y.-H. Wu, L.-X. Shi, Q.-P. Lin and Z.-N. Chen, *Dalton Trans.*, 2010, **39**, 8288–8295.
66 Selected examples: (*a*) K. A. McGee and K. R. Mann, *Inorg. Chem.*, 2007, **46**, 7800; (*b*) E. S. Andreiadis, D. Imbert,

J. Pécaut, A. Calborean, I. Ciofini, C. Adamo, R. Demadrille and M. Mazzanti, *Inorg. Chem.*, 2011, **50**, 8197; (*c*) M. Y. Wong, G.-H. Xie, C. Tourbillon, M. Sandroni, D. B. Cordes, A. M. Z. Slawin, I. D. W. Samuel and E. Zysman-Colman, *Dalton Trans.*, 2015, **44**, 8419.

67 F.-F. Chen, Z.-Q. Bian and C.-H. Huang, *Chin. J. Inorg. Chem.*, 2008, **24**, 1219.

68 (*a*) L.-G. Yang, A. von Zelewsky, H. P. Nguyen, G. Muller, G. Labat and H. Stoeckli-Evans, *Inorg. Chim. Acta*, 2009, **362**, 3853; (*b*) F. Blasberg, J. W. Bats, M. Wagner and H.-W. Lerner, *Acta Crystallogr., Sect. E: Struct. Rep. Online*, 2011, **67**, m1837.

69 H. J. Bolink, L. Cappelli, E. Coronado, A. Parham and P. Stössel, *Chem. Mater.*, 2006, **18**, 2778–2780.

70 N. M. Shavaleev, G.-H. Xie, S. Varghese, D. B. Cordes, A. M. Z. Slawin, C. Momblona, E. Ortí, H. J. Bolink, I. D. W. Samuel and E. Zysman-Colman, *Inorg. Chem.*, 2015, **54**, 5907–5914.